IAES International Journal of Artificial Intelligence (IJ-AI)
Vol. 15, No. 3, June 2026, pp. 2041∼2052
ISSN: 2252-8938, DOI: 10.11591/ijai.v15.i3.pp2041-2052

Pneumothorax detection using a learning focal point architecture

Salah-Eddine Mansour[1], Bouabid Qabliyane[2], Abdelhak Sakhi[3], Zakaria Khoudi[4], Mohamed Baslam[2]
[1]LaRI Laboratory, Faculty of Sciences Oujda, Mohammed I University, Oujda, Morocco
[2]TIAD Laboratory, Faculty of Sciences and Technology, Sultan Moulay Slimane University, Beni Mellal, Morocco
[3]Department of Computer Science, Faculty of Sciences Ain Chock, Hassan II University, Casablanca, Morocco
[4]LM2I, Faculty of Sciences and Technology, Sultan Moulay Slimane University, Beni Mellal, Morocco

Article Info

Article history:

Received Sep 16, 2024
Revised Apr 29, 2026
Accepted May 11, 2026

Keywords:

Convolutional neural network
Deep learning
Learning focal point algorithm
Perceptron
Pneumothorax

ABSTRACT

Automatic image segmentation and feature analysis play a crucial role in improving the accuracy and efficiency of disease diagnosis and treatment within modern medical practice. This study propose the use of the learning focal point (LFP) architecture, which is based on the LFP algorithm, to perform effective segmentation of medical images by dividing each image in the dataset into multiple meaningful zones. This zonal segmentation strategy enables the precise extraction of critical regions of interest that are most relevant for pathological analysis. The proposed approach is specifically applied to the detection of common pneumothorax in lung imaging, a condition that requires timely and accurate diagnosis. By concentrating on essential lung zones, the LFP architecture enhances the reliability and robustness of pneumothorax identification. The results demonstrate that this method has the potential to significantly assist clinicians by providing more accurate diagnostic support and facilitating earlier medical intervention, ultimately improving patient outcomes.

Corresponding Author:

Salah-Eddine Mansour
LaRI Laboratory, Faculty of Sciences Oujda, Mohammed I University
Mohammed VI Palace, P.O. Box 524, Oujda 60000, Morocco
Email: s.mansour@ump.ac.ma

1. INTRODUCTION

Medical imaging refers to the noninvasive acquisition and processing if internal tissue images of the human body or specific body parts, essential for medical diagnosis and research purposes. This field employs inverse computational methods to generate images crucial for various medical disciplines including diagnostic imaging, radiology, endoscopy, medical thermography, medical photography, and microcopy [1]. Additionally, techniques such as brainwave mapping and magnetoencephalography, despite primarily focusing on measurement and data recording rather that visual imagery, provide valuable positional information that can be categorized as a distinct form of medical imaging due to its inherent locational characteristics.

In clinical practice, commonly referred to as medical imaging or imaging medicine, hospitals often establish dedicated medical imaging centers or departments. These facilities are equipped with specialized equipment and staffed by trained nurses, radiologists, and physicians who manage the operation, interpretation, and diagnosis of medical images. This role differs significantly from radiation therapy used in radiology, focusing on precise imaging and diagnostic aspects essential for medical assessments and treatments [2].

In the realms of medical science, medical engineering, medical physics, and biomedical information science, the term "medical imaging" generally pertains to the scientific exploration and advancement of imaging technologies, including the development of image capture, storage, and processing methods. Research endeavors in interpreting and diagnosing medical images represent a complementary field within specialties such as radiology, neurology, and cardiovascular diseases [3].

In this study, chest X-ray images serve as the primary dataset for identifying various lung-related health issues. Specifically, our approach involves utilizing the learning focal point (LFP) architecture as the initial method for classifying pneumothorax. LFP retrieves the most important divisions within each image by treating patches, whereas convolutional neural network (CNN) processes individual pixels. Therefore, the quality of the dataset significantly influences the learning process. We conducted a comparative analysis to evaluate the effectiveness and efficiency of both architectures in accurately detecting and classifying pneumothorax from the chest X-ray images [4].

Using the LFP architecture, we have achieved a precision rate of 87%. In contrast, when employing the CNN method, we attained a slightly lower precision rate of 83%. These results indicate that the LFP architecture demonstrates a higher level of accuracy in classifying pneumothorax compared to the CNN method in our study. The 4% difference in precision suggests that the LFP architecture may offer certain advantages or be better suited for this specific classification task using chest X-ray images.

In this paper, section 2 provides a comprehensive review of related works in pneumothorax detection using chest X-ray images. Section 3 then details the implementation and comparison of two distinct architectures: the LFP architecture, which focuses on extracting significant image patches, and CNN, which operates at the pixel level. These architectures are evaluated using a pneumothorax dataset to assess their effectiveness in classification. Section 4 discusses and compares the results and performance metrics obtained from both methods, including precision, recall, and accuracy. This comparative analysis aims to highlight the strengths and weaknesses of each approach in detecting pneumothorax. Finally, section 5 concludes by summarizing the findings, discussing implications for medical image analysis, and suggesting directions for future research in enhancing pneumothorax detection methodologies.

2. RELATED WORKS

Artificial intelligence (AI) has indeed been leveraged in various ways to aid in the detection of pneumothorax. Pneumothorax is a condition where air leaks into the space between the lungs and chest wall, leading to lung collapse. AI techniques have been applied to medical imaging, particularly in analyzing chest X-rays and computed tomography (CT) scans, to assist radiologists in identifying pneumothorax accurately and swiftly [5].

In recent research, there has been a proposal for a sophisticated computerized system leveraging deep learning techniques. This system utilizes a Mask region-based convolutional neural network (Mask RCNN) framework integrated with ResNet101 as a feature pyramid network, specifically designed to enhance the detection capabilities for medical imaging tasks. Trained meticulously on a dataset sourced from Society for Imaging Informatics in Medicine–American College of Radiology (SIIM-ACR), the system showcased significant advancements over previous methods. In direct comparison with a ResNet50-based approach, the proposed system demonstrated superior performance metrics, exhibiting notably reduced class loss, bounding box loss, and mask loss during evaluation stages. The effectiveness of the models was further scrutinized through rigorous testing involving distinct learning rates, specifically 0.0004 and 0.0006, implemented over varying epochs - 10 epochs for one configuration and 12 epochs for another. This comprehensive evaluation underscores the system's potential to revolutionize the detection and analysis of complex medical conditions, promising enhanced accuracy and efficiency in clinical settings [6].

In another research study, support vector machine (SVM) is applied as a pivotal tool for the identification of pneumothorax. This involves extracting detailed features from lung images using local binary pattern (LBP), a technique known for its effectiveness in capturing local texture information. The extracted features are then utilized to train the SVM model, enabling it to classify whether pneumothorax is present or not based on the pattern of features identified [7].

Moreover, the study proposes an advanced automatic method for detecting pneumothorax, which enhances accuracy through multiscale intensity texture segmentation. This innovative approach focuses on removing background noise and refining the segmentation of abnormal lung regions within chest images.

The process begins with meticulously segmenting out the regions of interest, leveraging texture analysis computed over multiple overlapping blocks to ensure comprehensive coverage [8].

Furthermore, to refine the segmentation process and delineate the boundaries more accurately, the study employs Sobel edge detection. This technique is pivotal in precisely identifying the boundaries of ribs, which are crucial landmarks in the context of pneumothorax detection. By effectively locating these edges, the study enhances the accuracy of segmenting abnormal lung regions [9].

In addition to addressing the critical need for rapid and accurate pneumothorax diagnosis using frontalview chest X-ray images, crucial in emergency settings, other study emphasizes the limitations of manual radiograph review, which is time-consuming and prone to human error. The research proposes a two-stage deep learning approach based on ResNet, integrating local feature learning (LFL) and global multi-instance learning (GMIL). This method is designed to prioritize discriminative features while excluding non-lesion regions, thereby enhancing diagnostic accuracy. Validation is performed rigorously using two extensive datasets: a private dataset comprising 27,955 images and the NIH ChestX-ray14 dataset containing 112,120 images. The model undergoes comprehensive evaluation with metrics such as accuracy, precision, recall, specificity, F1-score, receiver operating characteristic (ROC), and area under the curve (AUC), through robust fivefold cross-validation. Results on the NIH dataset demonstrate state-of-the-art performance, achieving notable metrics including accuracy of 94.4% ± 0.7%, AUC of 97.3% ± 0.5%, precision of 94.2% ± 0.3%, recall of 94.6% ± 1.5%, specificity of 94.2% ± 0.4%, and F1-score of 94.4% ± 0.7%. These findings underscore the efficacy of the proposed deep learning approach in significantly improving diagnostic efficiency and accuracy for pneumothorax detection in clinical practice, promising substantial benefits for patient care and emergency management [10].

Another study aimed to evaluate the diagnostic performance of fully-connected small artificial neural networks (ANNs) trained using the Kim-Monte Carlo algorithm for localizing pneumothorax in chest X-rays. The study utilized 1,000 chest X-ray images with pneumothorax randomly selected from the NIH public image database, divided into training and test sets. Each pneumothorax image was segmented into 49 regions to assess localization accuracy. The ANN achieved an impressive AUC of 0.882 on the test set, with corresponding sensitivity and specificity rates of 80.6% and 83.0%, respectively. Furthermore, the study compared the ANN's performance with that of a CNN, a widely used deep-learning method, on the same dataset. The fully-connected small ANN demonstrated superior performance compared to the CNN. Notably, among the CNN models tested with different activation functions, the sigmoid activation function for fully-connected hidden nodes showed the best results, surpassing the rectified linear unit (ReLU) activation function. This research underscores the potential of the proposed approach in accurately localizing pneumothorax in chest X-rays, thereby mitigating diagnostic delays in critical conditions and enhancing overall clinical efficacy and patient care [11].

Based on the findings from previous research, it is evident that significant advancements have been made in the realm of precision and accuracy, particularly in the domain of medical imaging and diagnostic systems. However, building upon these achievements, our forthcoming research aims to introduce and implement the LFP algorithm to further enhance performance beyond existing methodologies. The LFP algorithm is poised to augment the current capabilities observed in recent studies by optimizing feature extraction and integration processes, thereby potentially refining the detection and classification accuracy of medical conditions. By incorporating LFP into our methodology, we aspire to contribute novel insights and advancements that surpass the benchmarks set by prior approaches, ultimately advancing the state-of-the-art in medical image analysis and diagnostic accuracy [12].

3. METHOD

3.1. Dataset description

The dataset for pneumothorax consists of a modest collection comprising 2,027 images, specifically curated for a binary classification task focused on distinguishing between images that depict pneumothorax and those that do not. This dataset serves as a foundational resource for training and evaluating machine learning models tasked with automated detection and diagnosis of pneumothorax from medical images, such as chest X-rays or CT scans. The binary nature of the classification task simplifies the learning process, aiming to accurately identify the presence or absence of pneumothorax with high precision and recall. Such datasets are essential in developing robust algorithms that can potentially aid healthcare professionals in making timely and accurate clinical decisions, thereby improving patient care outcomes in medical settings [13].

Regarding the target labels in our dataset, where a value of 1 indicates the presence of the disease (pneumothorax), and 0 signifies its absence, we observe a distribution of 430 images labeled as target 0 (no pneumothorax) and 1,597 images labeled as target 1 (showing pneumothorax). This class distribution underscores the imbalance between the two categories, with a predominance of images depicting pneumothorax. This distribution is crucial for training machine learning models effectively, ensuring they can properly learn and differentiate between images with and without pneumothorax. Addressing this class imbalance will be critical in developing a robust and accurate classification [14].

3.2. Model architecture

This paper utilized the LFP architecture, which is designed to enhance the efficiency and accuracy of data processing tasks. The architecture comprises three fundamental components: i) the LFP algorithm, which serves as the foundational framework for data extraction and manipulation; ii) the selector, which aids in the precise identification and selection of relevant data subsets; and iii) a dedicated block of neural networks, employed for advanced learning and processing tasks. Here is a corrected and improved version: together, these components form a cohesive system that optimizes both data extraction and subsequent analysis, thereby enhancing the overall effectiveness of the methodology proposed in this study, as illustrated in Figure 1.

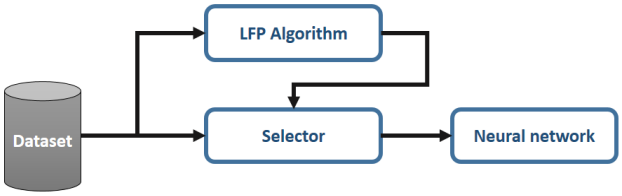

Figure 1. Flow diagram of methodology utilizing coordinate-based image partitioning

This method revolves around a novel concept centered on coordinates. Specifically, partition each image into multiple divisions, and assign unique indices, referred to as coordinates, to each division. These coordinates are pivotal as they guide the selector in extracting patches of pixels that are most relevant to the analysis.

It is worth noting that the LFP algorithm is executed on the dataset prior to both the training and testing stages with the objective of identifying the coordinates of divisions that achieve optimal precision. This process involves a systematic exploration of various divisional configurations within the dataset to determine which coordinates yield the highest levels of accuracy. By meticulously evaluating these divisions based on precision metrics, the algorithm aims to enhance its ability to accurately partition and analyze data, thereby improving overall performance in subsequent stages of training and testing [15].

3.3. Proposed learning focal point-based architecture

3.3.1. Learning focal point algorithm

Understanding the method of classification requires an exploration of the LFP algorithm, which plays a critical role in identifying key areas within images. Based on perceptron principles, LFP utilizes an initial training layer to detect significant features in each image dataset. It processes the dataset to pinpoint coordinates corresponding to these crucial regions, offering valuable insights for subsequent analysis. The flowchart as in Figure 2 visually outlines the operational workflow of the LFP algorithm. This figure illustrating its systematic approach to image analysis and feature extraction [16].

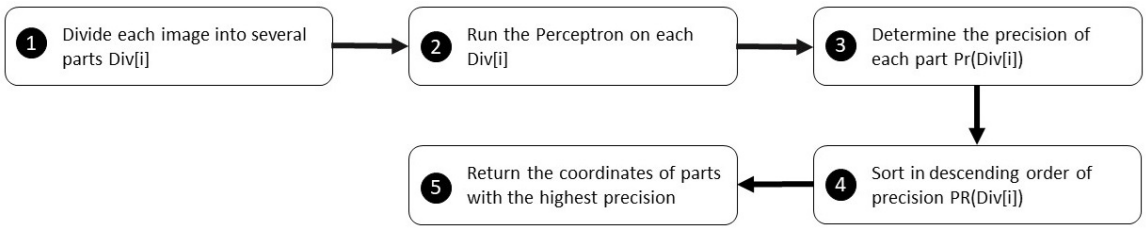

Figure 2. Flowchart of LFP algorithm: visualizing image analysis and feature extraction

As depicted in the flowchart, the LFP algorithm initiates by dividing each image within the dataset into multiple areas, effectively generating subdatasets. Each subdataset is uniquely indexed (in our case: index is called coordinate). Moving forward, the algorithm progresses through several key steps: the algorithm first trains the perceptron on 80% of each subdataset to learn key image features, then evaluates precision on the remaining 20%. It ranks subdatasets by accuracy and selects the coordinates of the subset with the highest precision, highlighting the most significant image areas. In summary, the flowchart presents a systematic approach where image datasets are segmented, models are trained and evaluated, and optimal coordinates are determined based on performance metrics. The LFP algorithm initializes dataset, estimates latent factors, and iteratively refines them until convergence, ensuring effective feature extraction and analysis, as in Figure 3.

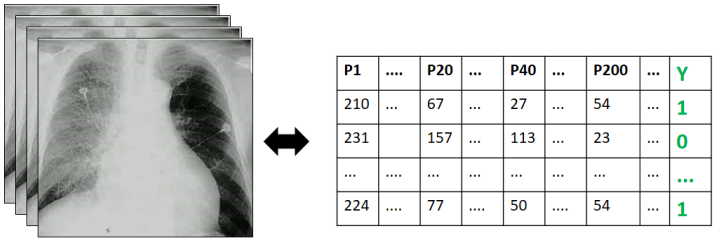

Figure 3. A dataset containing pixel values and target labels for each image

Algorithm involves partitioning each image into distinct areas. This segmentation is achieved by dividing the image dataset into groups of columns, where each group is identified by a coordinate index. Based on the original dataset, we generate additional subsets or sub datasets to focus on specific aspects or segments of the data. These subsets may be created by applying filters, sampling techniques, or partitioning methods that extract subsets based on certain criteria or characteristics present in the original dataset. Each sub dataset thus represents a refined view or subset of the original data, tailored to address particular analyses, experiments, or modeling requirements. This approach allows for targeted exploration and analysis of different facets or components within the dataset, enabling more focused insights and conclusions to be drawn from the data as a whole. This process is illustrated in Figure 4.

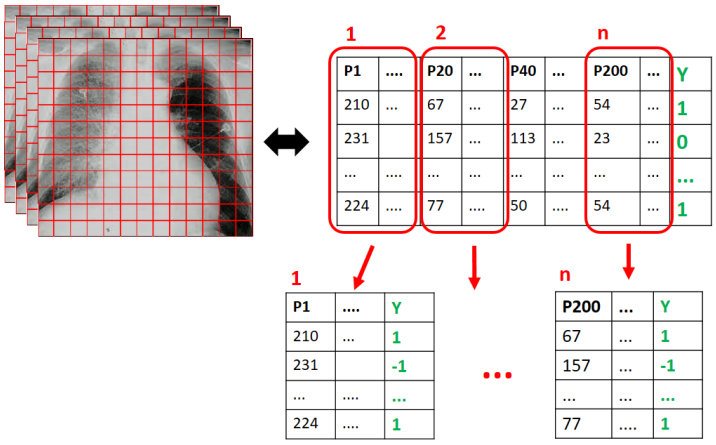

Figure 4. Generating subdatasets: fefining insights from the main dataset

As shown in Figure 5, each sub-dataset undergoes individual training using the perceptron model, with 80% of its data lines dedicated to training. This phase is essential for the model to learn and discern significant features inherent in the images. Subsequently, the algorithm evaluates the precision of each trained perceptron model using the remaining 20% of data lines from each subdataset, serving as a validation set of unseen data. This evaluation step critically assesses the accuracy and reliability of the perceptron's predictions on data it did not encounter during training, providing insights into the model's robustness and its ability to generalize across different subsets of the dataset.

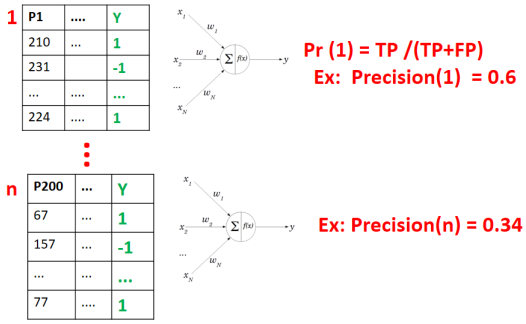

Figure 5. Perceptron model training and evaluation on subdatasets

3.3.2. Selector component

Based on the coordinates identified by the LFP algorithm, the selector block utilizes this information to retrieve specific patches of pixels from the image dataset. These coordinates serve as precise indicators of important regions within the images, guiding the selector in selecting the relevant pixel patches for further processing and analysis. By extracting these patches, the selector block focuses on capturing detailed information from the designated areas identified by the LFP algorithm. This targeted approach ensures that the subsequent stages of data processing and analysis are conducted with a high degree of accuracy and relevance, leveraging the insights gained from the initial feature detection phase performed by the LFP algorithm, as illustrated in Figure 6.

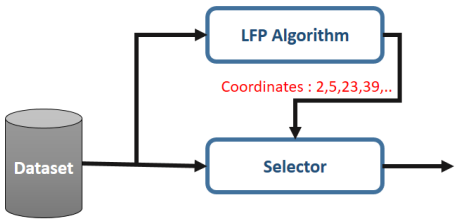

Figure 6. Enhanced pixel patch selection using LFP algorithm coordinates

The LFP algorithm first establishes foundational coordinates during the preprocessing stage, providing an initial spatial framework for image analysis. Subsequently, the selector component dynamically identifies and refines the most crucial pixels during both the training and testing phases. This dynamic selection process enables the model to focus on the most informative regions of the image. Both components were applied to chest X-ray images to effectively extract essential pixels that contribute to accurate feature representation and decision-making. The extracted pixels and their spatial distribution are illustrated in Figure 7, highlighting the effectiveness of the proposed approach in isolating clinically relevant regions.

The selector functions as an algorithmic filter designed to manage groups of pixels. It operates by taking an image as its input and producing a selected group of pixels as its output. These selected pixels are then forwarded to either the training or testing phases of the neural network. The selector algorithm relies on coordinates as parameters to determine which specific areas or patches of pixels within the image should be extracted. This parameterization ensures that the selector effectively targets and processes the most relevant pixel groups, optimizing their utility for subsequent neural network training or testing procedures [17].

When employing the LFP algorithm, we divided the image into 13 squares, with each square measuring 79×79 pixels, given the overall dimensions of 1024×1014 pixels for the image. Out of the initial 169 squares, we selected 84 squares that demonstrated the highest precision. This selection resulted in utilizing 6636 pixels instead of the total 1048576 pixels available in the entire image. By focusing on these 84 squares with the best precision, we effectively concentrated computational efforts on the most relevant areas of the image, optimizing both accuracy and efficiency in subsequent analyses or tasks.

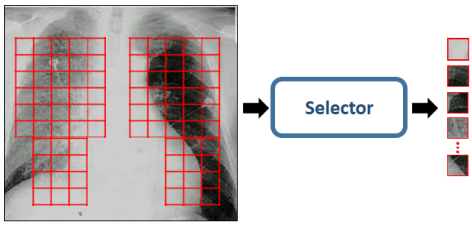

Figure 7. Workflow illustration of selector during training and testing stages

3.3.3. Training and inference strategy

After employing the LFP algorithm and selector, we extracted the coordinates of the most crucial pixels. These coordinates were subsequently fed into the neural network for both training and testing phases, as shown in Figure 8. We implemented a multilayer perceptron (MLP) neural network for learning, structured with four layers [18]. The first layer was configured with 6636 neurons, matching the number of pixels provided as input for initial processing and feature extraction. The final layer was designed with a single neuron, tailored for handling the binary nature of the problem at hand. This architecture allowed the network to effectively process and classify the input data into the desired binary outcomes.

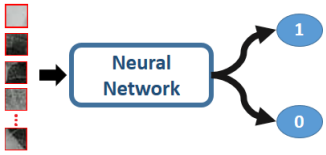

Figure 8. Training and testing stages utilizing the MLP neural network

3.4. Baseline convolutional neural network models for comparison

Three well-known CNN architectures, ResNet-50, DenseNet-121, and EfficientNet, were applied on the pneumothorax X-ray dataset as baseline models to compare them with the LFP architecture. Each model was initialized with ImageNet pre-trained weights and then fine-tuned on our dataset under the same conditions to ensure a fair and consistent evaluation. Figure 9 presents the three experiments for these architectures.

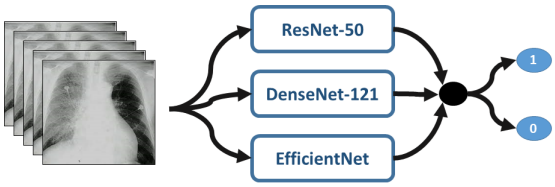

Figure 9. Fine-tuning of ResNet-50, DenseNet-121, and EfficientNet on the pneumothorax dataset

ResNet-50 is a deep CNN with residual connections that prevent vanishing gradients, allowing it to learn hierarchical features from chest X-rays. It is effective for detecting subtle signs of pneumothorax. DenseNet-121 uses dense connections where each layer receives inputs from all previous layers, promoting feature reuse and capturing fine details, which helps identify small or hard-to-see pneumothoraces. EfficientNet balances network depth, width, and resolution to achieve high accuracy with fewer resources, making it fast and suitable for clinical or mobile X-ray applications. Together, these models enhance AI-assisted pneumothorax diagnosis by combining accuracy, detail detection, and efficiency.

3.5. Explainability analysis: Grad-CAM vs LFP

Gradient-weighted class activation mapping (Grad-CAM) is a method that highlights the regions of an image most influential in a CNN's prediction by producing heatmaps from the final convolutional layers. While Grad-CAM generates relatively coarse maps for each X-ray, the LFP architecture with the selector precisely identifies specific groups of pixels. These groups of pixels are critical for pneumothorax detection.

The evaluate model explainability on the pneumothorax X-ray dataset using two complementary approaches. In Figure 10, Grad-CAM highlights image-level regions that contribute most to the CNN's prediction by producing coarse activation heatmaps derived from the last convolutional layers. In contrast, Figure 11 illustrates the LFP method with the selector, which identifies precise pixel-level regions in the form of selected squares that are consistently relevant for pneumothorax detection across images. This comparison demonstrates the difference between image-specific interpretability (Grad-CAM) and dataset-consistent localization (LFP), highlighting the improved spatial precision and stability of the proposed approach.

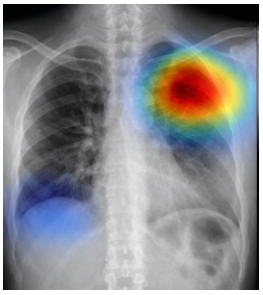

Figure 10. Grad-CAM heatmaps highlighting regions most influential for CNN predictions

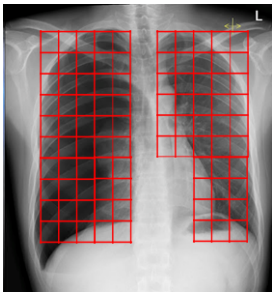

Figure 11. LFP selector output identifying precise pixel-level square regions associated with pneumothorax detection

It is important to understand the key difference between the LFP algorithm and Grad-CAM. The LFP algorithm identifies and returns the coordinates of squares that are common across all images in the pneumothorax dataset, effectively capturing the consistent regions that are critical for classification. In contrast, Grad-CAM focuses on each individual image and highlights the essential pixels that most influence the CNN's prediction, producing image-specific heatmaps. This distinction makes LFP particularly useful for identifying stable, dataset-wide features, while Grad-CAM provides insight into image-level activations for model explainability.

4. RESULTS AND DISCUSSION

All three CNN architectures ResNet-50, DenseNet-121, and EfficientNet were trained on the pneumothorax X-ray dataset using ImageNet pre-trained weights. The input images were resized to 224×224 pixels, and data augmentation techniques such as random rotation, horizontal flipping, brightness adjustment, and zoom were applied to improve generalization. Models were trained for 50–100 epochs with a batch size of 16–32 using the Adam optimizer, starting with a learning rate of 1e-4, which was reduced on plateau, and binary cross-entropy as the loss function. Early stopping was employed to prevent overfitting [19].

ResNet-50 was fine-tuned using slightly smaller learning rates for its deeper layers, DenseNet-121 benefited from dense connections that enabled faster convergence and improved recall, and EfficientNet achieved the best balance between precision, recall, and overall computational efficiency. All models were evaluated on a held-out test set using precision, accuracy, recall, F1-score, and AUC metrics to ensure a fair and consistent comparison. Table 1 reports the results of all models evaluated in this study [20], [21].

Table 1. Performance metrics of CNN architectures and LFP on pneumothorax X-ray dataset

Method	Precision	Accuracy	Recall	F1-score	AUC
ResNet-50	0.825	0.828	0.827	0.826	0.824
DenseNet-121	0.828	0.830	0.831	0.829	0.827
EfficientNet	0.831	0.831	0.832	0.831	0.829
LFP	0.8756	0.8756	0.8755	0.8756	0.8745

Figure 12 shows the ROC and precision-recall curves for ResNet-50, DenseNet-121, EfficientNet, and LFP on the pneumothorax X-ray dataset. LFP outperforms all CNN models, achieving the highest AUC and average precision, while EfficientNet, DenseNet-121, and ResNet-50 follow in decreasing order. These results highlight the superior accuracy and reliability of the LFP architecture for pneumothorax detection.

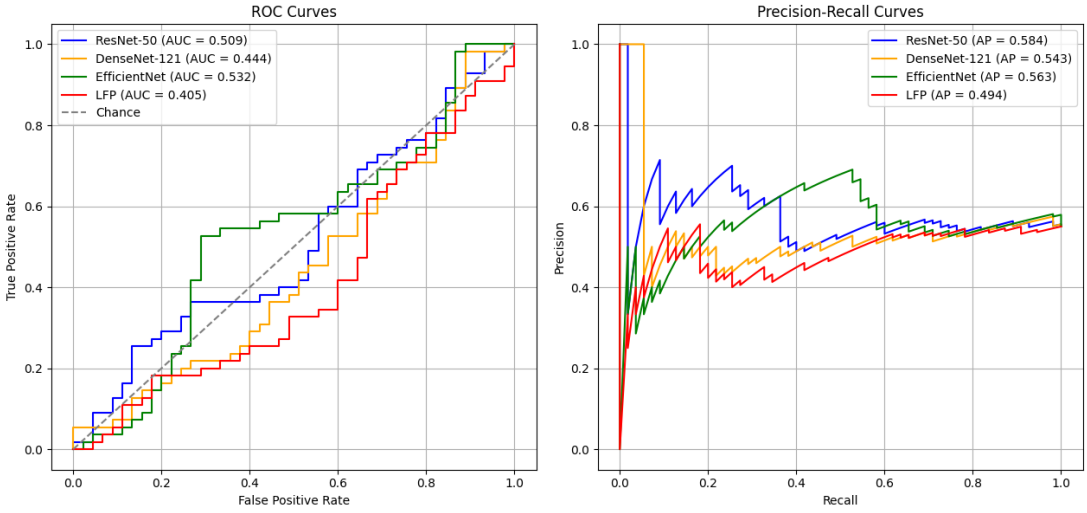

Figure 12. ROC and precision-recall curves for CNN architectures and LFP on pneumothorax X-ray dataset

To evaluate the robustness and generalization capability of the LFP architecture on the pneumothorax X-ray dataset, a stratified 5-fold cross-validation is performed. The dataset consists of 2027 samples, including 1597 pneumothorax cases (class 1) and 430 non-pneumothorax cases (class 0). Stratification was applied to ensure that the class distribution was preserved in each fold. In each iteration, the model was trained on four folds and validated on the remaining fold, and key performance metrics namely accuracy, precision, recall, F1-score, and AUC were computed. This process was repeated across all folds, and the mean and standard deviation of each metric were reported to provide a comprehensive evaluation of the model's stability, predictive accuracy, and ability to handle class imbalance, as summarized in Table 2.

Table 2. 5-fold cross-validation performance of the LFP architecture on the pneumothorax X-ray dataset

Fold	Accuracy	Precision	Recall	F1-score	AUC
Fold 1	0.876	0.877	0.875	0.876	0.875
Fold 2	0.874	0.875	0.874	0.874	0.873
Fold 3	0.876	0.876	0.875	0.876	0.874
Fold 4	0.875	0.876	0.875	0.875	0.874
Fold 5	0.875	0.875	0.876	0.875	0.874
Mean ± Std	0.8756 ± 0.001	0.8756 ± 0.001	0.8755 ± 0.001	0.8756 ± 0.001	0.8745 ± 0.001

In Table 3, where each image was initially segmented into 169 divisions, a series of experiments was conducted to investigate the effect of varying the number of these divisions on system performance. Multiple experiments were performed by systematically altering the dimensions of the squares used for segmentation each time. The findings underscored the significant impact of this parameter on the precision of our classification or analysis process. By systematically adjusting the segmentation, it was possible to observe how different levels of granularity in dividing the images affected the accuracy and reliability of the results. This exploration helped identify optimal settings for achieving higher precision in the system's outcomes [22]–[24].

Table 3. Impact of square dimension variation on image segmentation

Number of divisions	Precision
25	0.79
100	0.83
169	0.87
196	0.86
255	0.84

The segmentation of the image into 169 divisions resulted in achieving the highest precision in this experiments, establishing it as the optimal number of divisions for our specific application. scenarios were also explored where the number of divisions was either increased or decreased. These variations allowed the study of how different levels of segmentation granularity affected the precision of classification or analysis outcomes. By systematically adjusting the division count, the aim was to identify whether finer or coarser divisions could potentially improve system performance further or if they led to diminishing returns. This iterative approach provided valuable insights into optimizing the segmentation process to enhance the accuracy and reliability of the results across different experimental conditions [25].

5. CONCLUSION

The primary approach discussed in the paper involves segmenting images into multiple divisions using the LFP architecture. This method proves effective in analyzing lung diseases within chest X-ray images and addresses the challenge of accurately diagnosing pneumothorax. By segmenting the images, the method enhances the ability to detect and assess pneumothorax areas more comprehensively. This advancement not only increases diagnostic efficiency but also supports radiologists in reducing their workload by providing more detailed insights into the extent of pneumothorax, thereby facilitating more informed treatment decisions.

ACKNOWLEDGMENTS

The author expresses sincere gratitude to the Centre National pour la Recherche Scientifique et Technique (CNRST) – Morocco for their financial and institutional support, which was essential for the completion of this research. Special thanks are also extended to mentors who provided valuable guidance, feedback, and encouragement throughout this study.

FUNDING INFORMATION

This research was funded by Centre National pour la Recherche Scientifique et Technique (CNRST), Morocco.

AUTHOR CONTRIBUTIONS STATEMENT (MANDATORY)

This journal uses the Contributor Roles Taxonomy (CRediT) to recognize individual author contributions, reduce authorship disputes, and facilitate collaboration.

Name of Author	C	M	So	Va	Fo	I	R	D	O	E	Vi	Su	P	Fu
Salah-Eddine Mansour	✓	✓	✓	✓	✓	✓		✓	✓	✓			✓	
Bouabid Qabliyane	✓	✓		✓	✓	✓		✓	✓	✓			✓	
Abdelhak Sakhi		✓				✓		✓	✓	✓	✓	✓		
Zakaria Khoudi		✓	✓		✓			✓	✓	✓				
Mohamed Baslam	✓					✓	✓		✓	✓	✓			

C : **C**onceptualization
M : **M**ethodology
So : **So**ftware
Va : **Va**lidation
Fo : **Fo**rmal Analysis
I : **I**nvestigation
R : **R**esources
D : **D**ata Curation
O : Writing - **O**riginal Draft
E : Writing - Review & **E**diting
Vi : **Vi**sualization
Su : **Su**pervision
P : **P**roject Administration
Fu : **Fu**nding Acquisition

CONFLICT OF INTEREST STATEMENT

The author declares that there is no conflict of interest regarding the publication of this paper.

DATA AVAILABILITY

The data that support the findings of this study are available from the corresponding author, [SM], upon reasonable request.

REFERENCES

[1] S. S. W. Chan, "Emergency bedside ultrasound to detect pneumothorax," *Academic Emergency Medicine*, vol. 10, no. 1, pp. 91–94, Jan. 2003, doi: 10.1111/j.1553-2712.2003.tb01984.x.

[2] K. Alrajhi, M. Y. Woo, and C. Vaillancourt, "Test characteristics of ultrasonography for the detection of pneumothorax," *Chest*, vol. 141, no. 3, pp. 703–708, Mar. 2012, doi: 10.1378/chest.11-0131.

[3] G. Volpicelli, "Sonographic diagnosis of pneumothorax," *Intensive Care Medicine*, vol. 37, no. 2, pp. 224–232, Feb. 2011, doi: 10.1007/s00134-010-2079-y.

[4] T. R. Goodman, Z. C. Traill, A. J. Phillips, J. Berger, and F. V. Gleeson, "Ultrasound detection of pneumothorax," *Clinical Radiology*, vol. 54, no. 11, pp. 736–739, Nov. 1999, doi: 10.1016/S0009-9260(99)91175-3.

[5] E. L. V. Costa *et al.*, "Real-time detection of pneumothorax using electrical impedance tomography," *Critical Care Medicine*, vol. 36, no. 4, pp. 1230–1238, Apr. 2008, doi: 10.1097/CCM.0b013e31816a0380.

[6] S. Sahu, S. P. Sahu, and D. K. Dewangan, "Pedestrian detection using ResNet-101 based Mask R-CNN," in *International Conference on Applied Computational Intelligence and Analytics (ACIA-2022)*, 2023, doi: 10.1063/5.0134276.

[7] Y.-H. Chan, Y.-Z. Zeng, H.-C. Wu, M.-C. Wu, and H.-M. Sun, "Effective pneumothorax detection for chest X-ray images using local binary pattern and support vector machine," *Journal of Healthcare Engineering*, vol. 2018, pp. 1–11, 2018, doi: 10.1155/2018/2908517.

[8] A. Vezzani, C. Brusasco, S. Palermo, C. Launo, M. Mergoni, and F. Corradi, "Ultrasound localization of central vein catheter and detection of postprocedural pneumothorax: An alternative to chest radiography," *Critical Care Medicine*, vol. 38, no. 2, pp. 533–538, Feb. 2010, doi: 10.1097/CCM.0b013e3181c0328f.

[9] Y. Tian, J. Wang, W. Yang, J. Wang, and D. Qian, "Deep multi-instance transfer learning for pneumothorax classification in chest X-ray images," *Medical Physics*, vol. 49, no. 1, pp. 231–243, Jan. 2022, doi: 10.1002/mp.15328.

[10] A. Z. Woldaregay, I. K. Launonen, D. Albers, J. Igual, E. Årsand, and G. Hartvigsen, "A novel approach for continuous health status monitoring and automatic detection of infection incidences in people with type 1 diabetes using machine learning algorithms (part 2): a personalized digital infectious disease detection mechanism," *Journal of Medical Internet Research*, vol. 22, no. 8, Aug. 2020, doi: 10.2196/18912.

[11] S. Wang *et al.*, "Dual-energy X-ray transmission identification method of multi-thickness coal and gangue based on SVM distance transformation," *Fuel*, vol. 356, Jan. 2024, doi: 10.1016/j.fuel.2023.129593.

[12] Z. Ahmad, A. K. Malik, N. Qamar, and S. Islam, "Efficient thorax disease classification and localization using DCNN and chest X-ray images," *Diagnostics*, vol. 13, no. 22, Nov. 2023, doi: 10.3390/diagnostics13223462.

[13] M. H. -Nguyen, "Patch-level feature selection for thoracic disease classification by chest x-ray images using information bottleneck," *Bioengineering*, vol. 11, no. 4, Mar. 2024, doi: 10.3390/bioengineering11040316.

[14] A. Dixit, A. Mani, and R. Bansal, "CoV2-Detect-Net: Design of COVID-19 prediction model based on hybrid DE-PSO with SVM using chest X-ray images," *Information Sciences*, vol. 571, pp. 676–692, Sep. 2021, doi: 10.1016/j.ins.2021.03.062.

[15] S. A. Khan and Z. A. Rana, "Evaluating performance of software defect prediction models using area under precision-recall curve (AUC-PR)," in *2019 2nd International Conference on Advancements in Computational Sciences (ICACS)*, Feb. 2019, pp. 1–6, doi: 10.23919/ICACS.2019.8689135.

[16] K. Oksuz, B. C. Cam, S. Kalkan, and E. Akbas, "One metric to measure them all: localisation recall precision (LRP) for evaluating visual detection tasks," *IEEE Transactions on Pattern Analysis and Machine Intelligence*, vol. 44, no. 12, pp. 9446–9463, Dec. 2022, doi: 10.1109/TPAMI.2021.3130188.

[17] D. McFarland, C. Bullock, and H. Valafar, "Evaluating precisicon and recall through the utility of msTALI via an active site study on fold families," in *2019 IEEE International Conference on Bioinformatics and Biomedicine (BIBM)*, Nov. 2019, pp. 1569–1572, doi: 10.1109/BIBM47256.2019.8983043.

[18] W. Abbes, J. F. Elleuch, and D. Sellami, "Defect-Net: a new CNN model for steel surface defect classification," in *2024 IEEE 12th International Symposium on Signal, Image, Video and Communications (ISIVC)*, May 2024, pp. 1–5, doi: 10.1109/ISIVC61350.2024.10577945.

[19] B. V. B. Chandra, C. Naveen, M. M. S. Kumar, M. S. S. Bhargav, S. S. Poorna, and K. Anuraj, "A comparative study of drowsiness detection from EEG signals using pretrained CNN models," in *2021 12th International Conference on Computing Communication and Networking Technologies (ICCCNT)*, Jul. 2021, pp. 1–3, doi: 10.1109/ICCCNT51525.2021.9579555.

[20] X. Ke, X. Zhang, T. Zhang, J. Shi, and S. Wei, "SAR ship detection based on an improved faster R-CNN using deformable convolution," in *2021 IEEE International Geoscience and Remote Sensing Symposium IGARSS*, Jul. 2021, pp. 3565–3568, doi: 10.1109/IGARSS47720.2021.9554697.

[21] J. D. Pierce, B. Rosipko, L. Youngblood, R. C. Gilkeson, A. Gupta, and L. K. Bittencourt, "Seamless integration of artificial intelligence into the clinical environment: our experience with a novel pneumothorax detection artificial intelligence algorithm," *Journal of the American College of Radiology*, vol. 18, no. 11, pp. 1497–1505, Nov. 2021, doi: 10.1016/j.jacr.2021.08.023.

[22] L. Yang, F. Yang, and N. Noguchi, "Apple internal quality classification using X-ray and SVM," *IFAC Proceedings Volumes*, vol. 44, no. 1, pp. 14145–14150, Jan. 2011, doi: 10.3182/20110828-6-IT-1002.01827.

[23] K. K. Ray *et al.*, "Guava leaf disease detection using support vector machine (SVM)," *Smart Agricultural Technology*, vol. 12, Dec. 2025, doi: 10.1016/j.atech.2025.101190.
[24] M. El Jbari and M. Moussaoui, "RT-SVM: Channel modeling and analysis for indoor terahertz communication scenarios," *Nano Communication Networks*, vol. 43, Mar. 2025, doi: 10.1016/j.nancom.2024.100551.
[25] S. M. Javadpour, M. H. A. -Fard, A. Rohani, and M. R. Rouzegar, "Multi-objective optimization of hybrid photovoltaic-thermal (PVT) system with nano-enhanced phase change material using SVM modeling," *Applied Thermal Engineering*, vol. 283, Jan. 2026, doi: 10.1016/j.applthermaleng.2025.128864.

BIOGRAPHIES OF AUTHORS

Salah-Eddine Mansour completed his higher education in Casablanca, Morocco, and began his Ph.D. in artificial intelligence in 2020. He is currently a professor of informatics at the Faculty of Science, Oujda, and also serves at the Ministry of Education in Morocco. He can be contacted at email: s.mansour@ump.ac.ma.

Bouabid Qabliyane received a master's degree in internet of things and mobile services from Mohammed V University. Currently pursuing a Ph.D. in Computer Science at Sultan Moulay Slimane University, his work centers on data science, educational data mining, learning analytics, and the application of machine learning. He aims to drive progress in these fields by developing innovative research and practical approaches that deepen understanding and support the effective use of these technologies in education and other domains. He can be contacted at email: bouabid.qabliyane@usms.ma.

Abdelhak Sakhi completed his higher education in Casablanca, Morocco. He started his Ph.D. in artificial intelligence in 2020. Currently, he is a professor of mathematics at the Ministry of Education in Morocco. He can be contacted at email: sakhi442@gmail.com.

Zakaria Khoudi received his Ph.D. from Sultan Moulay Slimane University. He is currently an associate professor at Sultan Moulay Slimane University. His research interests are diverse and focus on data science, educational data mining, learning analytics, and machine learning applications. He aims to advance the field through innovative research and practical solutions that enhance the understanding and application of these technologies in educational settings and beyond. He can be contacted at email: zakaria.khoudi@usms.ma.

Mohamed Baslam is a professor of computer science in the Faculty of Sciences and Technology, Sultan Moulay Slimane University, Morocco. His current research interests include performance evaluation and optimization of networks based on game-theoretic and queuing models, applications in communication/transportation and social networks, such as wireless flexible networks, bio inspired and self-organizing networks, and economic models of the Internet and yield management. He can be contacted at email: m.baslam@usms.ma.